

Structural heterogeneity of apoB-containing serum lipoproteins visualized using cryo-electron microscopy

Rik van Antwerpen,^{1,*} Michael La Belle,[†] Edita Navratilova,^{*} and Ronald M. Krauss[†]

Department of Biochemistry,^{*} University of Arizona, Tucson, AZ 85721, and Ernest Orlando Lawrence Berkeley National Laboratory,[†] University of California, Berkeley, CA 94720

Abstract Cryo-electron microscopy was used to analyze the structure of lipoprotein particles in density gradient subfractions of human very low density lipoprotein (VLDL), intermediate density lipoprotein (IDL), and low density lipoprotein (LDL). Lipoproteins from a normolipidemic subject with relatively large and buoyant LDL (pattern A) and from a subject with a predominance of small dense LDL (pattern B) were compared. Projections of VLDL in vitreous ice were heterogeneous in size, but all were circular with a relatively even distribution of contrast. Selected projections of LDL, on the other hand, were circular with a high density ring or rectangular with two high density bands. Both circular and rectangular LDL projections decreased in average size with increasing subfraction density, but were found in all of 10 density gradient subfractions, both in pattern A and in pattern B profiles. Preparations of total IDL contained particles with the structural features of VLDL as well as particles resembling LDL. IDL particles resembling LDL were observed in specific density gradient subfractions in the denser region of the VLDL–IDL density range. Within the group of IDL particles resembling LDL considerable heterogeneity was observed, but no structural features specific for the pattern A or pattern B lipoprotein profile were recognized. **■** The observed structural heterogeneity of the apolipoprotein B-containing serum lipoproteins may reflect differences in the composition of these particles that may also influence their metabolic and pathologic properties.—van Antwerpen, R., M. La Belle, E. Navratilova, and R. M. Krauss. **Structural heterogeneity of apoB-containing serum lipoproteins visualized using cryo-electron microscopy.** *J. Lipid Res.* 1999. 40: 1827–1836.

Supplementary key words VLDL • IDL • LDL • low density lipoprotein

The human lipoproteins that contain apolipoprotein B-100 (apoB) [i.e., very low density lipoprotein (VLDL), intermediate density lipoprotein (IDL), and low density lipoprotein (LDL)] play critical roles in the serum transport of triacylglycerol and cholesteryl esters (1). VLDL is synthesized and secreted by the liver as a triacylglycerol-rich particle, and subsequent hydrolysis of VLDL-associated triacylglycerol by lipoprotein lipase converts VLDL to IDL at the luminal surface of vascular endothelial cells. Continued delipidation of IDL by both lipoprotein lipase and he-

patic lipase activity further converts IDL to LDL, which contains mainly cholesteryl esters in its hydrophobic core. During the lipolytic conversion of VLDL to LDL, apoB undergoes a conformational change that allows LDL to bind to the LDL receptor. This ultimately results in the removal of the lipoprotein particle from the circulation (1).

Recent studies indicate that the traditional VLDL, IDL, and LDL density classes contain different lipoprotein subspecies with distinct biochemical properties and metabolic fates (2). Turnover studies have suggested that the VLDL density class consists of at least two subclasses that contain lipoprotein particles of different average size (3–5). Both the synthesis and catabolism of these two subclasses appear to be regulated independently (3–5). In addition, VLDL subfractions with defined compositional differences have been isolated using affinity chromatography (6, 7).

Heterogeneity has also been observed in the IDL and LDL density classes. Total IDL contains at least two subclasses with different metabolic fates (8, 9), while the LDL density class consists of multiple subclasses with particles that differ in size, density, lipid composition, antioxidant content, electrical charge, and sensitivity to protease treatment (10–17). It has been demonstrated that several LDL subclasses differ in their affinity for the LDL receptor (18–24).

The possible relevance of various lipoprotein subclasses in the development of atherosclerosis is illustrated by studies on the heterogeneity of LDL. Based on LDL subclass distribution, individuals can be classified as having mostly large and buoyant LDL (pattern A) or predominantly small and dense LDL (pattern B) (10–12). The pattern B lipoprotein profile is associated with an up to 3-fold increased risk of developing coronary artery disease (25–27). Additional studies indicate that specific

Abbreviations: VLDL, very low density lipoprotein; IDL, intermediate density lipoprotein; LDL, low density lipoprotein; Cryo-EM, cryo-electron microscopy; GGE, gradient gel electrophoresis; EM, electron microscope.

¹ To whom correspondence should be addressed at current address: Department of Biochemistry and Molecular Biophysics, Virginia Commonwealth University, Medical College of Virginia Campus, Richmond, VA 23298.

VLDL and IDL subclasses may be involved in the development of atherosclerosis as well (25, 28). Both the metabolic heterogeneity of apoB-containing serum lipoproteins and the suspected heterogeneity in their atherogenic potential are thought to originate from structural differences in the apolipoprotein moieties. However, very little is known about the arrangement and conformation of apolipoprotein molecules in the various VLDL, IDL, and LDL particles.

Recent studies indicate that the spatial distribution of the apolipoprotein moiety on the lipoprotein surface can be visualized using cryo-electron microscopy (cryo-EM) (29–31). We therefore hypothesized that the metabolic heterogeneity of apoB-containing serum lipoproteins may correlate with a structural heterogeneity that can be observed using cryo-EM. To test this hypothesis, we analyzed the structure of lipoprotein particles in VLDL, IDL, and LDL density gradient subfractions. Our results reveal major structural differences between VLDL and LDL, as well as extensive structural heterogeneity within the IDL and LDL density classes.

MATERIALS AND METHODS

Subjects

ApoB-containing serum lipoproteins were isolated from a subject with relatively large and buoyant LDL (pattern A lipoprotein profile) and from a subject with a predominance of relatively small and dense LDL (pattern B lipoprotein profile). Plasma lipid concentrations for the pattern A subject were 77 mg/dl triglyceride, 168 mg/dl total cholesterol, 57 mg/dl HDL cholesterol, 96 mg/dl LDL cholesterol; the pattern B subject had plasma values of 147 mg/dl triglyceride, 159 mg/dl total cholesterol, 28 mg/dl HDL cholesterol, and 102 mg/dl LDL cholesterol. This study was approved by the Human Subjects Committee of the University of Arizona Health Sciences Center.

Lipoprotein isolation

After an overnight fast, blood samples were drawn into Vacutainers containing 1 mg of EDTA per ml, and cells were pelleted by low-speed centrifugation (2000 *g*, 4°C). Trolox (10 μ m), a water-soluble vitamin E analog, was added to plasma to prevent oxidation of lipoproteins during isolation.

VLDL ($d < 1.006$ g/ml), IDL ($1.006 < d < 1.019$ g/ml), and LDL ($1.019 < d < 1.063$ g/ml) were isolated by sequential ultracentrifugation (32), dialyzed into 150 mM NaCl (pH 7.4), 10 μ m Trolox, and stored under nitrogen at 4°C.

VLDL-IDL ($d < 1.019$ g/ml) was isolated by preparative ultracentrifugation (32), and subfractions were prepared by non-equilibrium density gradient ultracentrifugation as previously described (7). Briefly, the lipoprotein solution was dialyzed to a density of 1.21 g/ml, and 4.5-ml aliquots were added to 12 ml Beckman Ultraclear centrifuge tubes. These aliquots were then overlaid sequentially with 3 ml each of d 1.020 and 1.010 g/ml solutions, followed by 1.5 ml of a d 1.000 g/ml solution. The samples were centrifuged at 40,000 rpm for 6 h in a Beckman SW41 rotor at 17°C. After centrifugation, 8 fractions (four 1-ml fractions, followed by four 0.5-ml fractions) were collected and labeled 1 through 8 in order from the top of the centrifuge tube. Fractions were then dialyzed and stored as described above.

Compositional analysis

VLDL, IDL, and LDL protein concentrations were determined by a modification of the method of Lowry et al. (33) using BSA as the standard. Apolipoproteins B and E were measured using a standardized sandwich style ELISA (34), and detection with biotinylated antibodies (prepared from purified apoprotein-specific antisera), streptavidin-conjugated horseradish peroxidase, and *o*-phenylenediamine (Sigma Chemical Co., St. Louis, MO). Lipoprotein calibrators were standardized using CDC #1883 serum reference material (Center for Disease Control, Atlanta, GA) and pooled reference sera (Northwest Lipid Research Clinic, Seattle, WA). Phospholipids were measured by a standardized colorimetric method (35) using a phosphorus calibrator (Sigma Chemical Co.). Total cholesterol, unesterified cholesterol, and triglyceride were analyzed using enzymatic-endpoint reagent kits (Ciba-Corning Diagnostics Corp., Oberlin, OH), according to the manufacturer's instructions, on a Gilford Impact 500E auto analyzer (Ciba-Corning Diagnostics Corp.).

Gradient gel electrophoresis of lipoproteins

Lipoprotein particle diameters were determined by non-denaturing 2–14% polyacrylamide gradient gel electrophoresis (GGE) in 0.09 M Tris/0.08 M borate buffer (pH 8.3), 3 mM EDTA at 8–10°C (11, 36). Gels were stained for protein with Coomassie Brilliant Blue R-250 and scanned at 555 nm with a Transidyne RFT densitometer. LDL particle sizes were calculated from a calibration curve using high molecular weight standards (Pharmacia Biotech, Piscataway, NJ), 380 Å latex beads (Duke Scientific Corp., Palo Alto, CA), and lipoprotein calibrators stored frozen at –80°C. Plasma samples, stored at –80°C, were run in duplicate on each gel to serve as controls.

Cryo-electron microscopy

Cryo-EM samples were prepared by ultra-rapid freezing in liquid propane as described previously (29). Preparations were analyzed under low-dose conditions (ca. $10 e^-/\text{Å}^2$) at a temperature of –167°C using a Philips EM 420 Transmission Electron Microscope (Philips, Ramsey, NJ) and a Gatan, Model 626 Cryo-Transfer Device (Gatan Inc., Warrendale, PA). Recordings were taken at an instrument magnification of 29,000 \times , and at 1.6, 2.4, and 3.2 μ m underfocus.

EM measurement of lipoprotein particle diameters

Magnification settings of the electron microscope were calibrated using a standard diffraction grating replica (Ted Pella, Inc., Redding, CA). Photographic EM negatives were digitized on a flat bed scanner, and digitized images of the lipoprotein particles were further analyzed using the measuring tools of the computer program Adobe Photoshop, version 3.0 (Adobe Systems Inc., San Jose, CA). Averages and standard deviations of the measured parameters were calculated using the statistical functions of the computer program GraphPad Prism, version 1.03 (GraphPad Prism, San Diego, CA). Relevant parameters were measured on 50–200 particles for each point in the graphs. Photographic negatives were recorded randomly from areas in the preparation that were of suitable thickness, and all relevant projections in the photographic negative were measured. For determining the dimensions of LDL and small IDL particles, only circular projections with a distinct high density ring (face-on views of the observed structure) and rectangular projections with two distinct high density bands (edge-on views of the observed structure) were measured. By selecting only projections with well-defined high density rings or high density bands, inaccuracies in the measurements due to variations in the orientation of the particles were minimized.

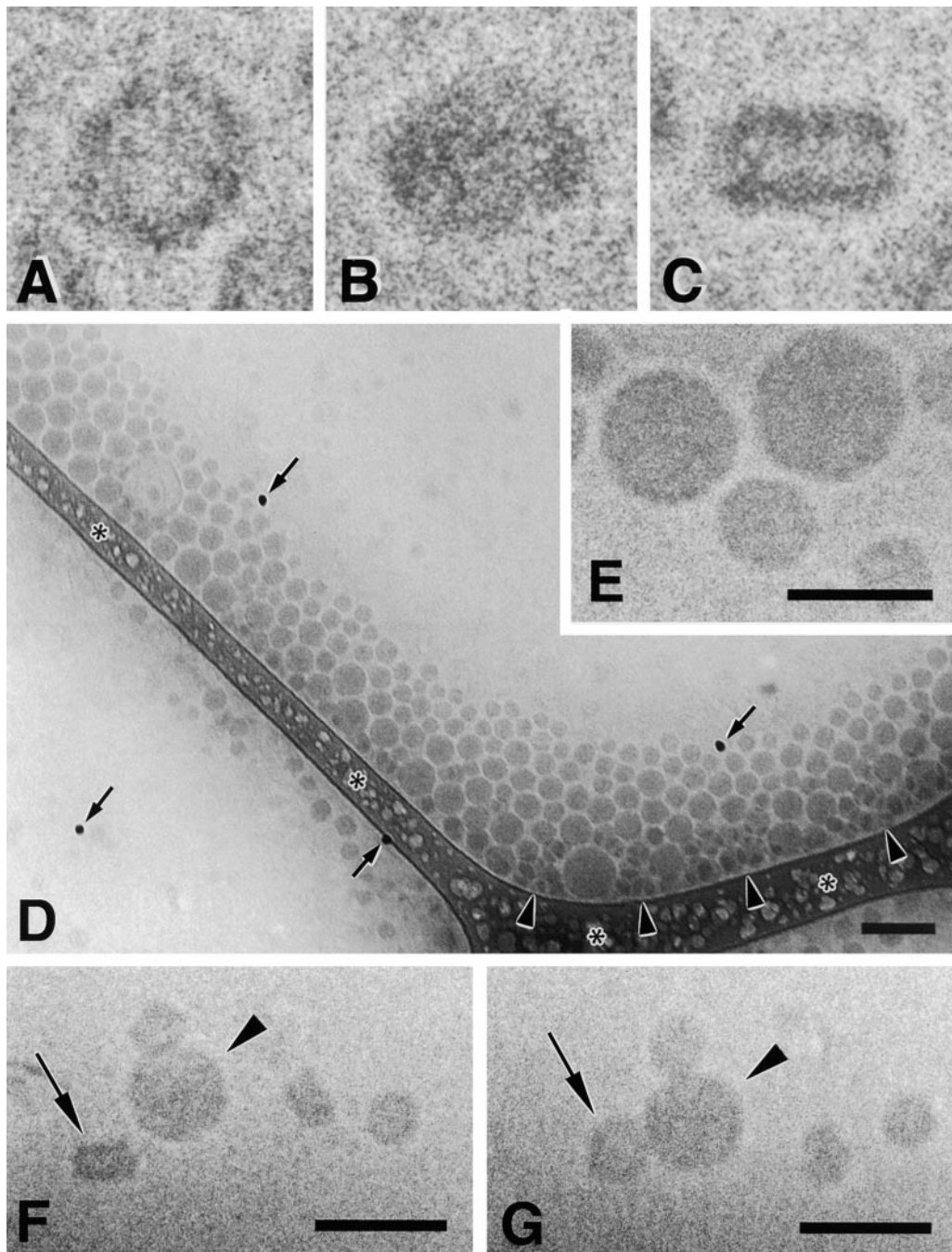


Fig. 1. A–C: Typical projections of normal LDL in vitreous ice. A: Circular projection with a ring of high density around the edge. B: Oval projection with increased density at the left and right tips of the projection. C: Rectangular projection with two high density bands parallel to the long axis of the projection. A–C are projections of three different particles; the width of these projections is ca. 21 nm. D–E: Cryo-electron micrographs of VLDL from a normolipidemic subject. D: Low magnification overview of a vitrified VLDL preparation. Asterisks indicate part of the lacy substrate that supports the suspended film of frozen VLDL solution. Arrows indicate colloidal gold particles that were included in the preparation as a focusing aid. In this particular area of the preparation, VLDL particles accumulated in the thickest part of the suspended film and were excluded from thinner parts in the center of the film. This localized accumulation is only seen occasionally, when the film of VLDL solution is extremely thin before vitrification. Arrowheads indicate areas where lipoprotein particles are superimposed in the two-dimensional plane of the micrograph. Scale bar represents 100 nm. E: High magnification cryo-electron micrograph of individual VLDL particles. Scale bar represents 50 nm. F–G: Cryo-electron micrographs of IDL from a normolipidemic subject. F: IDL particles in vitreous ice, viewed at an angle of -45° relative to the 0° plane of the sample holder. G: Same IDL particles as in F, viewed at an angle of $+45^\circ$ relative to the 0° plane of the sample holder. Note that tilting of the sample holder in the electron microscope resulted in a 90° difference in the viewing angle between F and G; the tilt axis runs horizontally across the figures. Scale bars in F and G represent 50 nm.

RESULTS

Total VLDL, IDL, and LDL

Cryo-electron micrographs of normal LDL in vitreous ice show a seemingly discoid structure with a double ring of high density around its perimeter (29, 31). Face-on views of this structure generate circular projections with a high density ring (Fig. 1A), while edge-on views generate rectangular projections with two high density bands (Fig. 1C). Views from angles between face-on and edge-on generate elliptical projections with somewhat increased density at the sharply curved ends (Fig. 1B).

The distinct projections shown in Fig. 1A–C were not

observed in cryo-EM preparations of total VLDL. All projections of VLDL in vitreous ice were roughly circular with a relatively even distribution of contrast (Fig. 1D,E). Diameters of the different VLDL projections were quite heterogeneous, ranging from ca. 18 to 50 nm, with a median diameter of 26 nm, and an average diameter of 27 ± 6.4 nm (\pm SD). Although the diameters of the smallest VLDL particles were within the size range of normal LDL, their projections did not have the rings or bands of high density seen in cryo-EM preparations of normal LDL.

In cryo-EM preparations of total IDL, relatively large particles resembling VLDL as well as smaller particles

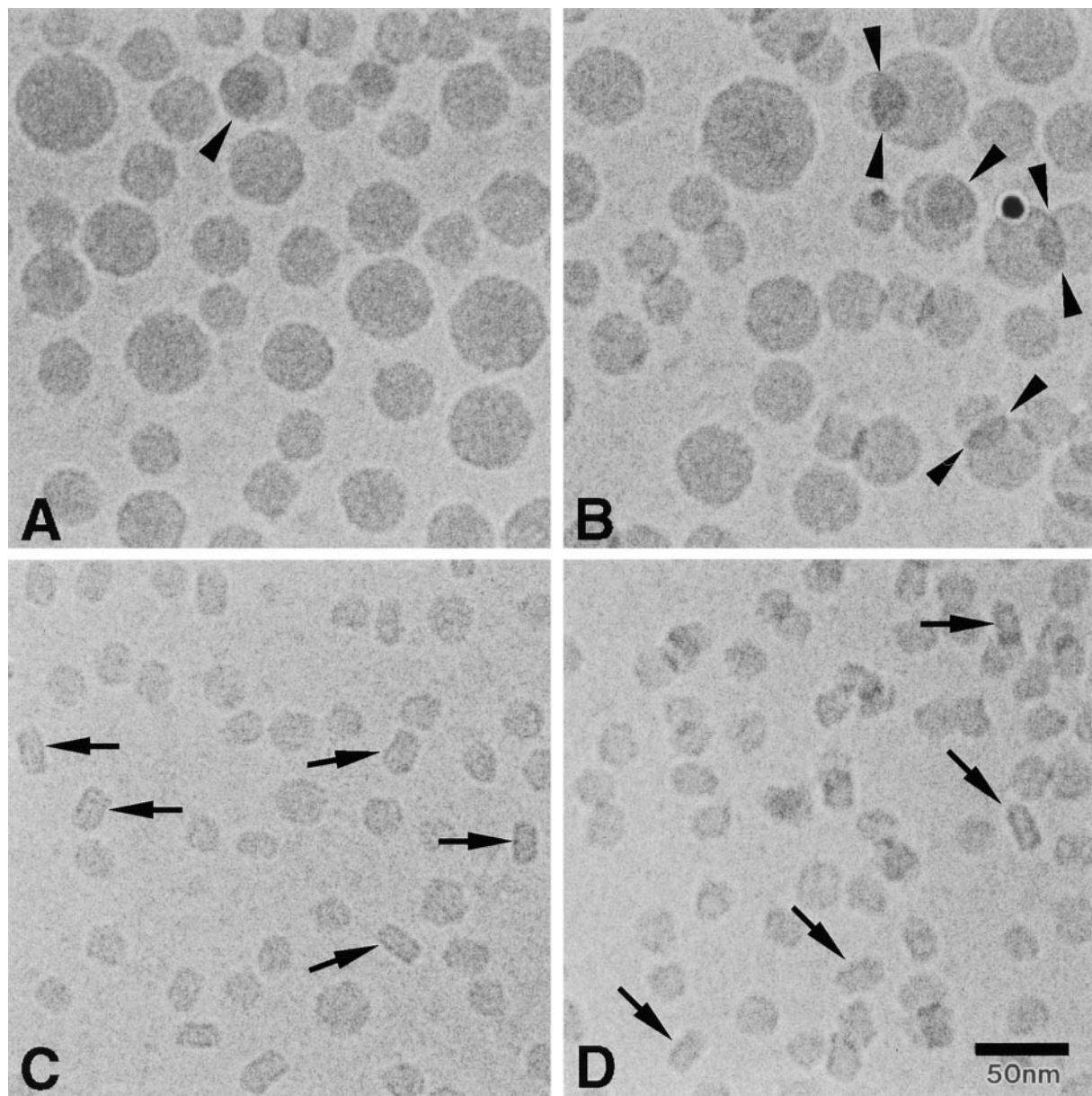


Fig. 2. Cryo-electron micrographs of lipoprotein particles from VLDL–IDL density gradient subfractions 1 and 6. A: subfraction 1, pattern A; B: Subfraction 1, pattern B; C: subfraction 6 pattern A; D: subfraction 6 pattern B. The black dot in B is one of the colloidal gold particles that were included in the preparation as a focusing aid. Arrowheads in A and B indicate areas where lipoprotein particles are imaged superimposed in the two-dimensional plane of the micrograph. Arrows in C and D indicate rectangular projections. Micrographs were taken at 2.4 μ m underfocus. Magnification 275,000 \times .

resembling LDL were detected (Fig. 1F,G). When VLDL-like particles were viewed from different angles (Fig. 1F,G, arrowhead), all resulting projections were circular, demonstrating that the observed structure is spherical. However, when LDL-like particles were viewed from different angles, rectangular projections with two high density bands (edge-on views) were “converted” to circular projections with a high density ring (face-on views) (Fig. 1F,G arrow) and vice versa. These observations established that total IDL from normolipidemic subjects contains at least two subclasses with distinct structural features.

VLDL-IDL density gradient subfractions

To further examine the possible existence of multiple structural subclasses of human VLDL and IDL, and to determine whether these subclasses might segregate according to density, we isolated eight VLDL-IDL subfractions using density gradient ultracentrifugation, and analyzed the different subfractions using cryo-EM. VLDL-IDL subfractions from subjects with either a pattern A or a pattern B lipoprotein profile were analyzed to determine whether structural differences exist between the corresponding lipoproteins of these two profiles. In both lipoprotein profiles, subfractions were labeled 1 through 8, with subfraction 1 having the lowest density (see materials and methods).

All cryo-EM projections of subfraction 1 were circular with a relatively even distribution of contrast, and no structural differences between projections of patterns A and B were recognized (Fig. 2A,B). The diameters of the different projections in subfraction 1 were quite heterogeneous (Fig. 3A), ranging from ca. 24 to 54 nm, with a median diameter of 31 nm, and an average diameter of 32.5 ± 6.6 nm (\pm SD) (for pattern A). The average diameter of lipoprotein particles decreased from 32.5 nm in subfraction 1 (pattern A) to 23.5 nm in subfraction 4 (pattern A) (Fig. 3A) without a significant change in the observed structure of the lipoproteins (results not shown). However, in cryo-electron micrographs of subfractions 5–8, rectangular projections such as those seen in preparations of normal LDL (Fig. 1C) and in preparations of total IDL (Fig. 1F) were recognized, both in pattern A and in pattern B lipoprotein profiles (Fig. 2C,D).

Considerable heterogeneity in both size and substructure was shown to exist within subfractions 5 through 8. Figure 4 illustrates this heterogeneity for lipoproteins from subfraction 6, pattern A. Particularly striking are differences in the width/height ratio (i.e., the aspect ratio) of different rectangular projections. The highest aspect ratio found in rectangular projections of subfraction 6 was 2.1 (Fig. 4, row 1), while the lowest aspect ratio found in this subfraction was 1.4 (Fig. 4, row 3). The average aspect ratio of rectangular projections in subfraction 6 was 1.85 ± 0.13 (\pm SD). Similar variations in the aspect ratios of rectangular projections were found in all subfractions 5–8 of both pattern A and B (Fig. 3B).

Structural heterogeneity was also observed in circular projections of subfractions 5–8 (Fig. 4). Some of those cir-

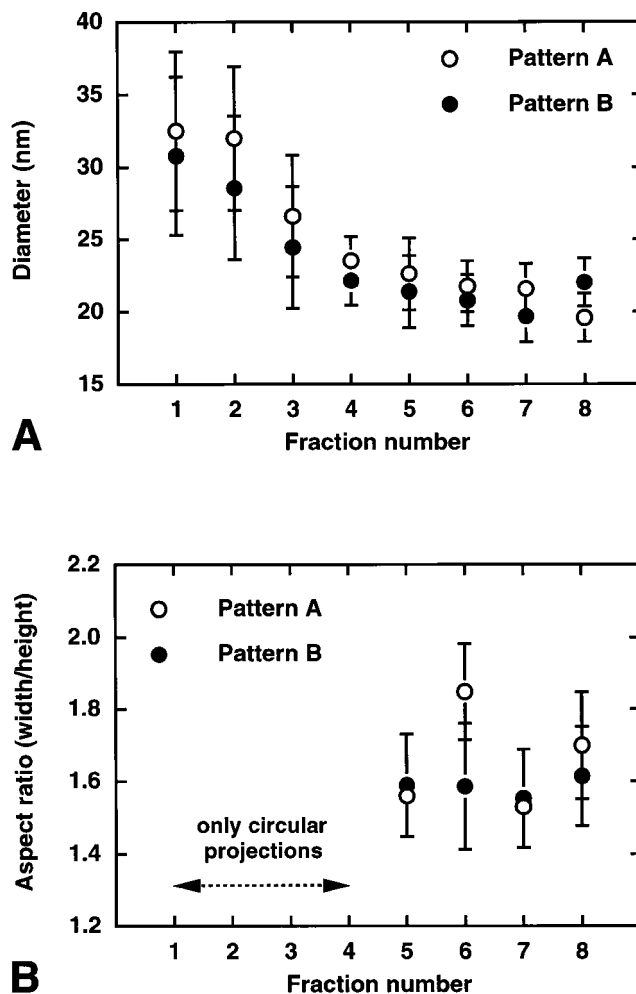


Fig 3. A: Average dimensions (\pm SD) of lipoprotein particles in VLDL-IDL density gradient subfractions of pattern A (open circles) and pattern B (closed circles), as measured in cryo-electron micrographs of the particles. Dimensions were measured on circular projections only. B: Average aspect ratios (\pm SD) of rectangular projections of lipoprotein particles in VLDL-IDL density gradient subfractions of pattern A (open circles) and pattern B (closed circles).

cular projections had a relatively even distribution of high density (Fig. 4, row 4), similar to the circular projections of subfraction 1 (Fig. 2A,B). Smaller circular projections often had a high density ring around their perimeter with a somewhat more translucent center (Fig. 4, row 6), similar to circular projections of LDL (Fig. 1A). Other circular projections were intermediate between the latter two types in both size and substructure (Fig. 4, row 5).

To determine whether focus adjustments of the electron microscope had an effect on the observed structures, we recorded images at underfocus settings of 1.6–3.2 μ m. Figure 4 demonstrates that a change in the underfocus setting of the electron microscope only led to alterations in the structural details of the lipoprotein images: in both rectangular and circular projections, the appearance of certain high density “domains” changed with the underfocus setting. Similarly, some rectangular projections of

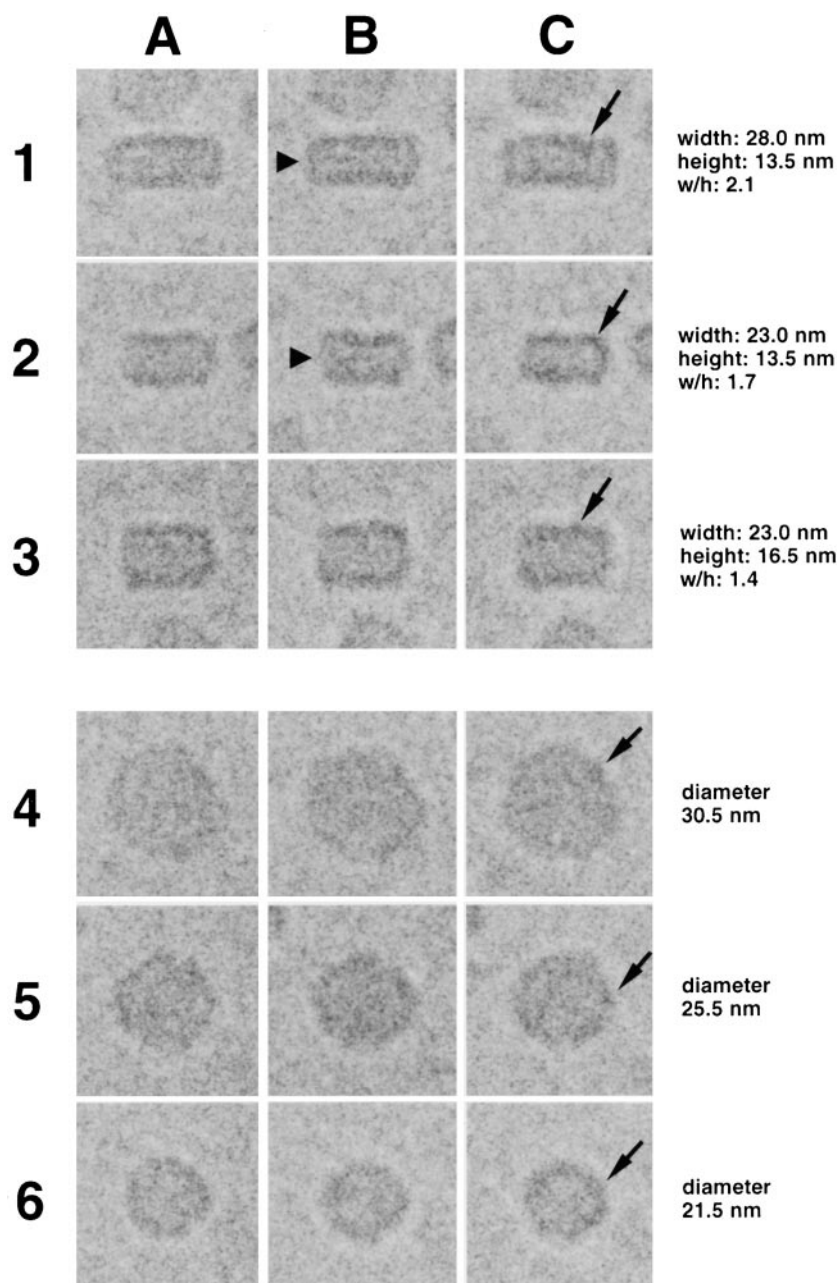


Fig. 4. Rows 1–3: Selected rectangular projections of three different lipoprotein particles from VLDL–IDL subfraction 6 (pattern A), recorded at underfocus settings of 1.6 μm (column A), 2.4 μm (column B), and 3.2 μm (column C). Rows 4–6: Selected circular projections of three different lipoprotein particles from VLDL–IDL subfraction 6 (pattern A), recorded at underfocus settings of 1.6 μm (column A), 2.4 μm (column B), and 3.2 μm (column C). Arrows indicate detailed high density features that change with the underfocus setting of the electron microscope. Arrowheads indicate a faint third band of high density that is only visible at specific underfocus settings.

subfractions 5–8 contained a faint third band of high optical density that was visible only at particular underfocus settings (Fig. 4, images 1B and 2B). However, the overall appearance of the circular projections with a high density ring and the rectangular projections with two high density bands did not change when the underfocus setting of the electron microscope was varied between 1.6 and 3.2 μm (Fig. 4).

The presence of rectangular projections in cryo-EM

preparations of subfractions 5–8 correlated with several compositional parameters of the lipoprotein particles. The ratios of triacylglycerol/apoB (w/w), triacylglycerol/cholesteryl ester (w/w), and apoC-III/apoB (molar ratio) were relatively high in VLDL–IDL subfractions 1–4, and lower in subfractions 5–8, both in pattern A and in pattern B lipoprotein profiles (**Table 1**). Comparison of cryo-EM data with the compositional data of Table 1 shows that rectangular projections occurred when the triacylglycerol/

TABLE 1. Compositional analysis of VLDL-IDL density gradient subfractions from pattern A and pattern B lipoprotein profiles

VLDL/IDL Subfraction	Pattern A				Pattern B			
	w/w TG/ApoB	w/w TG/CE	Molar Ratio		w/w TG/ApoB	w/w TG/CE	Molar Ratio	
			ApoE/B	ApoC-III/B			ApoE/B	ApoC-III/B
1	13.93	>30	0.228	41.28	11.21	18.78	0.096	32.84
2	11.40	7.56	0.229	32.10	5.79	4.92	0.072	23.45
3	14.55	10.71	0.341	35.12	5.56	2.53	0.097	20.87
4	7.22	3.33	0.234	20.24	3.21	1.13	0.080	14.70
5	3.70	1.79	0.118	10.67	2.38	0.65	0.093	11.72
6	1.62	0.59	0.078	4.46	1.40	0.44	0.072	8.33
7	0.69	0.28	0.039	2.19	1.17	0.44	0.061	6.84
8	0.61	0.26	0.042	2.23	1.13	0.28	0.085	8.19

Lipid and apolipoprotein composition of each density gradient subfraction was determined as described in Materials and Methods; TG, triacylglycerol; CE, cholesteryl ester; apo, apolipoprotein.

apoB ratio was lower than 3–4, the triacylglycerol/cholesteryl ester ratio was lower than 1–2, and the apoC-III/apoB molar ratio was lower than ca. 15. Despite the suggestion of some compositional differences between corresponding subfractions 5–8 from patterns A and B (Table 1), no obvious structural differences were observed between the corresponding lipoproteins.

LDL density gradient subfractions

To determine the possible existence of structural subclasses of LDL, and to determine whether these subclasses might segregate according to density, we isolated 10 LDL subfractions using density gradient ultracentrifugation, and analyzed the different subfractions using cryo-EM. LDL subfractions from a subject with a pattern A lipoprotein profile were compared with subfractions from a person with a pattern B profile.

Projections of LDL particles in vitreous ice decreased in size with increasing fraction density as shown in Fig. 5A. No significant differences were observed in the average diameter of particles in corresponding subfractions of patterns A and B. However, the average diameter of total LDL particles from the pattern A subject was 20.1 ± 1.7 nm (\pm SD), while the average diameter of total LDL particles from the pattern B subject was significantly smaller ($P < 0.0001$) with a value of 17.9 ± 1.5 nm (\pm SD). These observations are consistent with the established predominance of relatively large and buoyant LDL particles in the pattern A profile and the prevalence of small and dense LDL particles in the pattern B profile.

Circular projections with a high density ring and rectangular projections with two high density bands were observed in all LDL subfractions, from both pattern A and pattern B lipoprotein profiles. As in IDL subfractions, the aspect ratios (width/height) of rectangular LDL projections varied extensively within each subfraction (Fig. 5B). In addition, within each LDL subfraction, both the width and the height of rectangular projections varied widely (Figs. 5C–D). In Figs. 5C and 5D, the average widths and heights of rectangular LDL projections from each individual subfraction of patterns A and B are plotted against each other. The height of the rectangular projections in pattern A appeared to vary over a narrower range than the

height of pattern B projections, as reflected in the slopes of the linear fits of Figs. 5C and 5D.

As for VLDL-IDL images, a change in the underfocus setting of the microscope led to alterations in the structural details of the LDL images. However, the overall shape of the circular projections with a high density ring and the rectangular projections with two high density bands did not change when the underfocus setting of the electron microscope was varied between 1.6 and 3.2 μ m (results not shown, see also reference 29 for total LDL).

Figure 6 shows that relative LDL particle diameters measured by cryo-EM correlated well with relative diameters measured by GGE ($r^2 = 0.85$). However, cryo-EM data consistently gave smaller lipoprotein diameters. VLDL and IDL subfractions were too heterogeneous to allow a similar correlation analysis to be performed.

DISCUSSION

Many studies have demonstrated that cryo-EM can provide detailed information on the structure of supramolecular assemblies close to their native state (37, 38). A particular advantage of cryo-EM over conventional EM techniques is that the use of chemical fixatives or stains can be avoided, and samples can be analyzed in a hydrated state. Furthermore, during the preparation of vitrified cryo-EM samples, freezing rates (i.e., fixation rates) are fast enough to preserve characteristic features of lipid phases that exist above the phase transition temperature of the system (39, 40). Therefore, the structure of lipoprotein particles as observed in the present study is in all likelihood very close to the structure of the lipoproteins at room temperature, i.e., the temperature from which the samples were frozen.

The present cryo-EM study reveals major structural differences between human VLDL and LDL particles. While projections of VLDL in vitreous ice are all circular with a relatively even distribution of contrast (Figs. 1D,E and 2A,B), specific projections of LDL are either circular with a high density ring or rectangular with two high density bands (Figs. 1A–C). The typical distribution of high density in projections of LDL suggests that the protein moiety of LDL (i.e., apoB) is organized as a double ring around

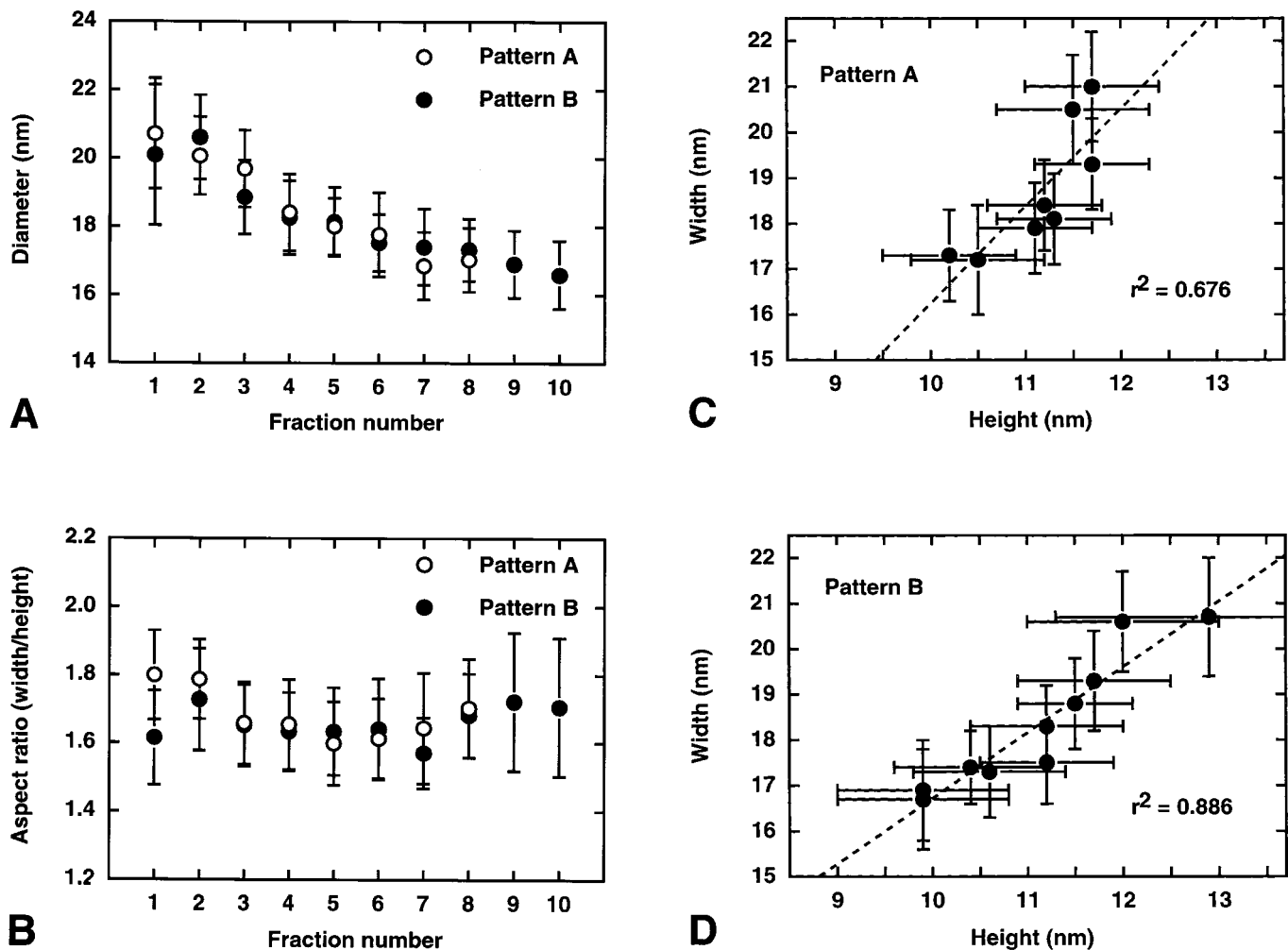


Fig. 5. A: Average dimensions (\pm SD) of lipoprotein particles in LDL density gradient subfractions of pattern A (open circles) and pattern B (closed circles), as measured in cryo-electron micrographs of the particles. Dimensions were measured on circular projections only. B: Average aspect ratios (\pm SD) of rectangular projections of lipoprotein particles in LDL density gradient subfractions of pattern A (open circles) and pattern B (closed circles). C: Average heights and widths of rectangular projections in density gradient subfractions of LDL, pattern A. D: Average heights and widths of rectangular projections in density gradient subfractions of LDL, pattern B.

the lipid core of the particle (29, 31). Similarly, the more homogeneous distribution of contrast in VLDL projections indicates that the protein moiety of VLDL is distributed more evenly across the lipoprotein surface. The structural difference between VLDL and LDL in vitreous ice may, therefore, reflect the dissociation of small apolipoproteins from the lipoprotein surface and/or the conformational change of apoB during the lipolytic conversion of VLDL to LDL (1).

A second important observation in the present study is that the IDL density class appears to contain at least two structural subclasses: one subclass with the overall features of VLDL (VLDL-like particles), and a second subclass that resembles LDL (LDL-like particles) (Figs. 1F,G). The presence of these two structural subclasses in cryo-EM preparations of total IDL correlates with non-denaturing gel electrophoresis studies in which two IDL subclasses with different biochemical properties were identified (8, 9).

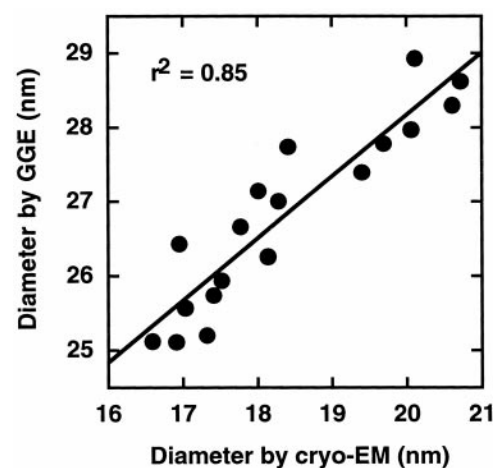


Fig. 6. Correlation of LDL particle diameters determined by non-denaturing polyacrylamide gradient gel electrophoresis (GGE) and cryo-electron microscopy (cryo-EM).

LDL-like particles were found in VLDL-IDL density gradient subfractions 5 through 8, both in pattern A and in pattern B lipoprotein profiles. Comparison of cryo-EM data with compositional analyses of these subfractions demonstrated that LDL-like cryo-EM projections are generated when the triacylglycerol/apoB ratio (w/w) was lower than 3–4, the triacylglycerol/cholesteryl ester ratio (w/w) was lower than 1–2, and the apoC-III/apoB molar ratio was lower than ca. 15. Any of these three compositional parameters may contribute to the observed structural difference between VLDL- and LDL-like particles. In addition, the size of the particles' lipid core may influence the observed structural features. However, the fact that some VLDL-like particles are smaller than some LDL-like particles suggests that parameters other than the volume of the lipid core play a role in the generation of LDL-like features.

Within the group of IDL particles that resemble LDL further heterogeneity was found. Specifically, the aspect ratios of various rectangular IDL projections, representing "edge-on" views of the observed structure, varied widely (Figs. 3B and 4). These observations suggest that the IDL density class may consist of multiple subclasses that can be defined by both particle size and aspect ratio. The existence of a variety of structural IDL subclasses is consistent with recent metabolic studies (reviewed in ref. 2).


The present study confirms many earlier studies in which LDL particle size was found to be inversely proportional to the density of the lipoproteins (Fig. 5). In our cryo-EM preparations, the average diameter of total LDL from the pattern A profile (20.1 ± 1.7 nm) was significantly larger than the average diameter of total LDL from the pattern B profile (17.9 ± 1.5 nm), thus confirming that the pattern B profile indeed contained a predominance of relatively small and dense LDL particles.

Although relative LDL size measurements by cryo-EM and GGE correlated well (Fig. 6), particle diameters determined by cryo-EM were consistently smaller than those determined by GGE. Previous work (41) has shown that measurement of lipoprotein size by different methods, each with its own potential limitations, can yield particle diameters differing by as much as 6.8 nm. These discrepancies are most likely due to differences in the physical behavior of the lipoprotein particles under different conditions of analysis. In the case of GGE, it is possible that interaction with the gel matrix during electrophoresis induces compression of the particle in the direction of migration, which would increase the apparent particle diameter. On the other hand, when measuring particle diameters on cryo-electron micrographs, the unevenness of the particle surface and the presence of background noise in the image introduces some subjectivity in choosing precise particle boundaries.

No obvious structural differences were found between LDL particles in corresponding density gradient subfractions of patterns A and B. Interestingly, even the smallest and densest LDL particles of the pattern B lipoprotein profile (present in subfractions 9 and 10) generated circu-

lar projections with a high density ring and rectangular projections with two high density bands. In an earlier cryo-EM study, we have shown that small dense LDL from an individual with severe hypertriglyceridemia [LDL subfraction 4.5 (17)] does not possess these specific structural features (31). Instead, distinct projections of LDL 4.5 are triangular or diamond-shaped (31). These observations suggest that further structural heterogeneity of the LDL density class exists in hypertriglyceridemic subjects.

As in IDL density gradient subfractions, highly variable aspect ratios of rectangular projections were found within density gradient subfractions of LDL. In all LDL subfractions, of both pattern A and pattern B lipoprotein profiles, these aspect ratios varied from ca. 1.5 to ca. 2.0. This demonstrates that within each LDL subfraction lipoprotein particles with considerable structural differences coexist. It remains to be established whether other purification methods, such as heparin- or immuno-affinity chromatography can be used to separate LDL particles with different size and aspect ratio.

The present study does not reveal obvious structural differences between the apoB-containing lipoproteins from the individuals with patterns A and B. However, it cannot be excluded that subtle structural differences between pattern A and pattern B lipoproteins do exist. Furthermore, either subtle or more obvious structural differences may only be found in a larger population of subjects. Future studies should, therefore, explore computer-assisted methods to rapidly and reliably quantify structural differences between various subclasses of the apoB-containing serum lipoproteins in vitreous ice. These methods can then be used to determine whether specific structural features observed with cryo-EM are related to an increased risk of developing atherosclerosis. 

The authors thank Dr. John Gilkey for stimulating discussions, and Mr. David Bentley from the Imaging Facilities of the Arizona Research Laboratories at the University of Arizona for providing equipment to perform the cryo-electron microscopy. The assistance of Patricia Blanche and the staff of the Donner Lipoprotein Analysis Laboratory in performing lipid and lipoprotein analyses is greatly appreciated. This work was supported by a FIRST Award from the National Institutes of Health (GM 50551), and by a Beginning Grant-in-Aid from the Arizona Affiliate of the American Heart Association (AZ 30-96) to RvA. Further support was provided by the National Institutes of Health Grant HL 14237 (Arteriosclerosis Specialized Center of Research), and by the National Institutes of Health Program Project Grant HL 18574 from the National Heart Lung and Blood Institute. Work at the Ernest Orlando Lawrence Berkeley National Laboratory was conducted through the U.S. Department of Energy under Contract No. DE-AC03-76SF00098.

Manuscript received 8 March 1999 and in revised form 9 July 1999.

REFERENCES

1. Gotto, A. M., Jr., H. J. Pownall, and R. J. Havel. 1986. Introduction to the plasma lipoproteins. *Methods Enzymol.* **128**: 3–41.
2. Packard, C. J., and J. Shepherd. 1997. Lipoprotein heterogeneity

- and apolipoprotein B metabolism. *Arterioscler. Thromb. Vasc. Biol.* **17**: 3542–3556.
3. Packard, C. J., A. Munro, A. R. Lorimer, A. M. Gotto, and J. Shepherd. 1984. Metabolism of apolipoprotein B in large triglyceride-rich very low density lipoproteins of normal and hypertriglyceridemic subjects. *J. Clin. Invest.* **74**: 2178–2192.
 4. Gaw, A., C. J. Packard, G. M. Lindsay, B. A. Griffin, M. J. Caslake, A. R. Lorimer, and J. Shepherd. 1995. Overproduction of small very low density lipoproteins (S_f 20–60) in moderate hypercholesterolemia: relationships between apolipoprotein B kinetics and plasma lipoproteins. *J. Lipid Res.* **36**: 158–171.
 5. Packard, C. J., A. Gaw, T. Demant, and J. Shepherd. 1995. Development and application of a multicompartmental model to study very low density lipoprotein subfraction metabolism. *J. Lipid Res.* **36**: 172–187.
 6. Campos, E., K. Nakajima, A. Tanaka, and R. J. Havel. 1992. Properties of an apoE-enriched fraction of triglyceride-rich lipoproteins isolated from human blood plasma with a monoclonal antibody to apolipoprotein B-100. *J. Lipid Res.* **33**: 369–380.
 7. Campos, E., S. Jackle, G. C. Chen, and R. J. Havel. 1996. Isolation and characterization of two distinct species of human very low density lipoproteins lacking apolipoprotein E. *J. Lipid Res.* **37**: 1897–1906.
 8. Musliner, T. A., C. Giotas, and R. M. Krauss. 1986. Presence of multiple subpopulations of lipoproteins of intermediate density in normal subjects. *Arteriosclerosis*. **6**: 79–87.
 9. Musliner, T. A., K. M. McVicker, J. F. Iosefa, and R. M. Krauss. 1987. Metabolism of human intermediate and very low density lipoprotein subfractions from normal and dysbetalipoproteinemic plasma. In vivo studies in the rat. *Arteriosclerosis*. **7**: 408–420.
 10. Shen, M. M., R. M. Krauss, F. T. Lindgren, and T. M. Forte. 1981. Heterogeneity of serum low density lipoproteins in normal human subjects. *J. Lipid Res.* **22**: 236–244.
 11. Krauss, R. M., and D. J. Burke. 1982. Identification of multiple subclasses of plasma low density lipoproteins in normal humans. *J. Lipid Res.* **23**: 97–104.
 12. Krauss, R. M., and P. Blanche. 1992. Detection and quantitation of LDL subfractions. *Curr. Opin. Lipidol.* **3**: 377–383.
 13. McNamara, J. R., D. M. Small, Z. Li, and E. J. Schaefer. 1996. Differences in LDL subspecies involve alterations in lipid composition and conformational changes in apolipoprotein B. *J. Lipid Res.* **37**: 1924–1935.
 14. La Belle, M., P. J. Blanche, and R. M. Krauss. 1997. Charge properties of low density lipoprotein subclasses. *J. Lipid Res.* **38**: 690–700.
 15. Tribble, D. L., J. J. M. van den Berg, P. A. Motchnik, B. N. Ames, D. M. Lewis, A. Chait, and R. M. Krauss. 1994. Oxidative susceptibility of low density lipoprotein subfractions is related to their ubiquinol-10 and alpha-tocopherol content. *Proc. Natl. Acad. Sci. USA*. **91**: 1183–1187.
 16. Goulinet, S., and M. J. Chapman. 1997. Plasma LDL and HDL subspecies are heterogeneous in particle content of tocopherols and oxygenated and hydrocarbon carotenoids. Relevance to oxidative resistance and atherogenesis. *Arterioscler. Thromb. Vasc. Biol.* **17**: 786–796.
 17. Chen, G. C., W. Liu, P. Duchateau, J. Allaart, R. L. Hamilton, C. M. Mendel, K. Lau, D. A. Hardman, P. H. Frost, M. J. Malloy, and J. P. Kane. 1994. Conformational differences in human apolipoprotein B-100 among subspecies of low density lipoproteins (LDL). Association of altered proteolytic accessibility with decreased receptor binding of LDL subspecies from hypertriglyceridemic subjects. *J. Biol. Chem.* **269**: 29121–29128.
 18. Knight, B. L., G. R. Thompson, and A. K. Soutar. 1986. Binding and degradation of heavy and light subfractions of low density lipoprotein by cultured fibroblasts and macrophages. *Atherosclerosis*. **59**: 301–306.
 19. Jakkola, O., T. Solakivi, S. Yla-Herttuala, and T. Nikkari. 1989. Receptor-mediated binding and degradation of subfractions of human plasma low-density lipoprotein by cultured fibroblasts. *Biochim. Biophys. Acta*. **1005**: 118–122.
 20. Swinkels, D. W., J. C. M. Hendriks, P. N. M. Demacker, and A. F. H. Stalenhoef. 1990. Differences in metabolism of three low density lipoprotein subfractions in Hep G2 cells. *Biochim. Biophys. Acta*. **1047**: 212–222.
 21. Nigon, F., P. Lesnik, M. Rouis, and M. J. Chapman. 1991. Discrete subspecies of human low density lipoproteins are heterogeneous in their interaction with the cellular LDL receptor. *J. Lipid Res.* **32**: 1741–1753.
 22. Chappell, D. A., G. L. Fry, M. A. Waknitz, and J. J. Berns. 1991. Ligand size as a determinant for catabolism by the low density lipoprotein (LDL) receptor pathway: a lattice model for LDL binding. *J. Biol. Chem.* **266**: 19296–19302.
 23. De Graaf, J., J. C. Hendriks, D. W. Swinkels, P. N. Demacker, and A. F. Stalenhoef. 1993. Differences in LDL receptor-mediated metabolism of three low density lipoprotein subfractions by human monocyte-derived macrophages: impact on the risk of atherosclerosis. *Artery*. **20**: 201–230.
 24. Campos, H., K. S. Arnold, M. E. Balestra, T. L. Innerarity, and R. M. Krauss. 1996. Differences in receptor binding of LDL subfractions. *Arterioscler. Thromb. Vasc. Biol.* **16**: 794–801.
 25. Krauss, R. M. 1987. Relationship of intermediate and low-density lipoprotein subspecies to risk of coronary artery disease. *Am. Heart J.* **113**: 578–582.
 26. Austin, M. A., J. L. Breslow, C. H. Hennekens, J. E. Buring, W. C. Willett, and R. M. Krauss. 1988. Low-density lipoprotein subclass patterns and risk of myocardial infarction. *J. Am. Med. Assoc.* **260**: 1917–1921.
 27. Krauss, R. M. 1994. Heterogeneity of plasma low-density lipoproteins and atherosclerosis risk. *Curr. Opin. Lipidol.* **5**: 339–349.
 28. Alaupovic, P., W. J. Mack, C. Knight-Gibson, and H. N. Hodis. 1997. The role of triglyceride-rich lipoprotein families in the progression of atherosclerotic lesions as determined by sequential coronary angiography from a controlled clinical trial. *Arterioscler. Thromb. Vasc. Biol.* **17**: 715–722.
 29. Van Antwerpen, R., and J. C. Gilkey. 1994. Cryo-electron microscopy reveals human low density lipoprotein substructure. *J. Lipid Res.* **35**: 2223–2231.
 30. Spin, J. M., and D. Atkinson. 1995. Cryoelectron microscopy of low density lipoprotein in vitreous ice. *Biophys. J.* **68**: 2115–2123.
 31. Van Antwerpen, R., G. C. Chen, C. R. Pullinger, J. P. Kane, M. LaBelle, R. M. Krauss, C. Luna-Chavez, T. M. Forte, and J. C. Gilkey. 1997. Cryo-electron microscopy of low density lipoprotein and reconstituted discoidal high density lipoprotein: imaging of the apolipoprotein moiety. *J. Lipid Res.* **38**: 659–669.
 32. Lindgren, F. T., L. C. Jensen, and F. T. Hatch. 1972. The isolation and quantitative analysis of serum lipoproteins. In *Blood Lipids and Lipoproteins*. J. Nelson, editor. John Wiley & Sons, Inc., New York, NY. 181–274.
 33. Markwell, M. A. K., S. M. Hass, L. L. Bieber, and N. E. Tolbert. 1978. A modification of the Lowry procedure to simplify protein determination in membrane and lipoprotein samples. *Anal. Biochem.* **87**: 206–210.
 34. Tijssen, P. 1985. Practice and theory of enzyme immunoassays. In *Laboratory Techniques in Biochemistry and Molecular Biology*, Vol. R. H. Burdon and P. H. van Knippenberg, editors. Elsevier Science Publishers B.V., Amsterdam. 345–347.
 35. Bartlett, G. R. 1959. Phosphorus assay in column chromatography. *J. Biol. Chem.* **234**: 466–471.
 36. Nichols, A. V., R. M. Krauss, and T. A. Musliner. 1986. Nondenaturing polyacrylamide gradient gel electrophoresis. *Methods Enzymol.* **128**: 613–626.
 37. Adrian, M., J. Dubochet, J. Lepault, and A. W. McDowell. 1984. Cryo-electron microscopy of viruses. *Nature*. **308**: 32–36.
 38. Dubochet, J., M. Adrian, J.-J. Chang, J.-C. Homo, J. Lepault, A. W. McDowell, and P. Schultz. 1987. Cryo-electron microscopy of vitrified specimens. *Q. Rev. Biophys.* **21**: 129–228.
 39. Siegel, D. P., L. Burns, H. Chestnut, and Y. Talmon. 1989. Intermediates in membrane fusion and bilayer/nonbilayer phase transitions imaged by time-resolved cryo-transmission electron microscopy. *Biophys. J.* **56**: 161–169.
 40. Frederik, P. M., M. C. A. Stuart, P. H. H. Bomans, W. M. Busing, K. N. J. Burger, and A. J. Verkleij. 1991. Perspective and limitations of cryo-electron microscopy. From model systems to biological specimens. *J. Microsc.* **161**: 253–262.
 41. Kahlon, T. S., G. L. Adamson, M. M. S. Shen, and F. T. Lindgren. 1982. Sedimentation equilibrium of human low density lipoprotein subfractions. *Lipids*. **17**: 323–330.